THE JOURNAL OF BIOLOGICAL CHEMISTRY
Vol. 278, No. 10, Issue of March 7, pp. 7891–7896, 2003

Printed in U.S.A.

Activity-Stability Relationships in Extremophilic Enzymes*

Received for publication, December 9, 2002
Published, JBC Papers in Press, January 2, 2003, DOI 10.1074/jbc.M212508200

Salvino D'Amico, Jean-Claude Marx, Charles Gerday, and Georges Feller‡

From the Laboratory of Biochemistry, University of Liège, Institute of Chemistry B6, B-4000 Liège-Sart Tilman, Belgium

Psychrophilic, mesophilic, and thermophilic α-amylases have been studied as regards their conformational stability, heat inactivation, irreversible unfolding, activation parameters of the reaction, properties of the enzyme in complex with a transition state analog, and structural permeability. These data allowed us to propose an energy landscape for a family of extremophilic enzymes based on the folding funnel model, integrating the main differences in conformational energy, cooperativity of protein unfolding, and temperature dependence of the activity. In particular, the shape of the funnel bottom, which depicts the stability of the native state ensemble, also accounts for the thermodynamic parameters of activation that characterize these extremophilic enzymes, therefore providing a rational basis for stability-activity relationships in protein adaptation to extreme temperatures.

Our planet harbors a huge number of harsh environments that are considered as "extreme" from an anthropocentric point of view, as far as temperature, pH, osmolarity, free water, or pressure are concerned. Nevertheless, these peculiar biotopes have been successfully colonized by numerous organisms, mainly extremophilic bacteria and archaea. As the curiosity of scientists stimulates the exploration of new environments, it seems that there is no "empty space" for life on Earth and, for instance, even the supercooled cloud droplets contain actively growing bacteria (1). Among the extremophilic microorganisms, those living at extreme temperatures have attracted much attention. Thermophiles have revealed the unsuspected upper temperature for life at about 113 °C (2, 3). Their enzymes have also demonstrated a considerable biotechnological potential such as the various thermostable DNA polymerases used in PCR that have boosted many laboratory techniques. At the other end of the temperature scale, metabolically active psychrophilic bacteria have been detected in liquid brine veins of sea ice at −20 °C (4). These cold-loving microorganisms face the thermodynamic challenge to maintain enzyme-catalyzed reactions and metabolic rates compatible with sustained growth near or below the freezing point of pure water (5, 6). Directed evolution experiments have highlighted that, in theory, cold activity of enzymes can be gained by several subtle adjustments of the protein structure (7). However, in natural cold environments, the consensus for the adaptive strategy is to take advantage of the lack of selective pressure for stable proteins for losing stability, therefore making the enzyme more mobile or flexible at temperatures that "freeze" molecular motions and reaction rates (8).

The crystal structures of extremophilic enzymes unambiguously indicate a continuum in the molecular adaptations to temperature. There is indeed a clear increase in the number and strength of all known weak interactions and structural factors involved in protein stability from psychrophiles to mesophiles (living at intermediate temperatures close to 37 °C) and to thermophiles (2, 9–11). Therefore, the same mechanism of molecular adaptation is involved in response to two distinct selective pressures, *i.e.* the requirement for stable protein structure and activity in thermophiles and the requirement for high enzyme activity in psychrophiles. This of course suggests intricate relationships between activity and stability in naturally evolved enzymes from these extremophiles. To date, these relationships have not been investigated in details mainly because most extremophilic enzymes were not analyzed in rigorously identical conditions. In the present work, we have investigated three structurally homologous α-amylases. The α-amylase from *Pseudoalteromonas haloplanktis* (AHA),[1] formerly *Alteromonas haloplanctis*, is the best characterized psychrophilic enzyme isolated from an Antarctic bacterium (12–14). Interestingly, its closest structural homologue is the pig pancreatic α-amylase (PPA), which is taken here as the mesophilic reference (15, 16). *Bacillus* species are able to colonize moderately thermophilic habitats, and *Bacillus amyloliquefaciens* secretes a thermostable α-amylase (BAA). This enzyme has been selected as the thermophilic counterpart because its unfolding is completed below 100 °C (17, 18), therefore allowing biophysical investigations at atmospheric pressure. The three-dimensional structures of these α-amylases can be superimposed, showing a strong conservation of the active site architecture, of the main secondary structures, and of the overall fold (14). However, the melting points of these proteins are markedly different: 45 °C for AHA, 65 °C for PPA, and 85 °C for BAA (12). Therefore, they constitute an adequate series of homologous enzymes for temperature adaptation studies.

EXPERIMENTAL PROCEDURES

Sources—The recombinant AHA was expressed in *Escherichia coli* at 18 °C and purified by DEAE-agarose, Sephadex G-100, and Ultrogel AcA54 column chromatography, as described previously (13). PPA and BAA were from Roche Molecular Biochemicals and Sigma, respectively.

Enzyme Assays—α-Amylase activity was recorded between 3 and 25 °C using 3.5 mM 4-nitrophenyl-α-D-maltoheptaoside-4,6-*O*-ethylidene as substrate and excess α-glucosidase as coupling enzyme in 100 mM Hepes, 50 mM NaCl, 10 mM $MgCl_2$, pH 7.2. Activities were recorded in a thermostated Uvikon 860 spectrophotometer (Kontron) and calculated on the basis of an absorption coefficient for 4-nitrophenol of 8,980 M^{-1} cm^{-1} at 405 nm; a stoichiometric factor of 1.25 was applied (13).

* This work was supported by the European Union (Grant CT970131), the Région Wallonne (Grants Bioval 981/3860, Bioval 981/3848, Initiative 114705), the FNRS Belgium (Grant 2.4515.00), and the Institut Polaire Français. The costs of publication of this article were defrayed in part by the payment of page charges. This article must therefore be hereby marked "*advertisement*" in accordance with 18 U.S.C. Section 1734 solely to indicate this fact.

‡ To whom correspondence should be addressed. Tel.: 32-4-366-33-43; Fax: 32-4-366-33-64; E-mail: gfeller@ulg.ac.be.

[1] The abbreviations used are: AHA, α-amylase from *P. haloplanktis*; PPA, α-amylase from pig pancreas; BAA, α-amylase from *B. amyloliquefaciens*; GdmCl, guanidinium chloride; DSC, differential scanning calorimetry; MOPS, 3-(*N*-morpholino)propanesulfonic acid.

Amylolytic activity recorded over a wide range of temperatures, up to 90 °C, was assayed by the dinitrosalicylic acid method (19) using 1% soluble starch as substrate in 100 mM Hepes, 50 mM NaCl, pH 7.2. Heat inactivation of enzymes incubated in 100 mM Hepes, 50 mM NaCl, pH 7.2, was recorded as a function of time at various temperatures. The residual activity of timed aliquots stored in ice for 1 h was measured by the standard assay at 25 °C.

Activation Parameters—Thermodynamic parameters of activation were calculated as described (20) using Equations 1–3,

$$\Delta G^{\#} = RT \times \left(\ln\frac{k_B T}{h} - \ln k\right) \quad \text{(Eq. 1)}$$

$$\Delta H^{\#} = Ea - RT \quad \text{(Eq. 2)}$$

$$\Delta S^{\#} = (\Delta H^{\#} - \Delta G^{\#})/T \quad \text{(Eq. 3)}$$

where k_B is the Bolzmann constant, h the Planck constant, E_a is the activation energy of the reaction, and R the gas constant.

Unfolding Recorded by Intrinsic Fluorescence—Fluorescence was recorded using an SML-AMINCO Model 8100 spectrofluorimeter (Spectronic Instruments) at an excitation wavelength of 280 nm (1-nm band pass) and at an emission wavelength of 350 nm (4-nm band pass). Heat-induced unfolding was recorded in 100 mM Hepes, 50 mM NaCl, pH 7.2, at a scan rate of 1 °C/min using a programmed water bath Lauda Ecoline RE306. GdmCl-induced unfolding was monitored at 20 °C after a 4-h incubation of the samples at this temperature in 30 mM MOPS, 50 mM NaCl, 1 mM $CaCl_2$, pH 7.2. Data were normalized using the pre- and post-transition baseline slopes as described (21). Least squares analysis of ΔG values as a function of GdmCl concentrations allowed the estimation of the conformational stability in the absence of denaturant, ΔG_{H_2O}, according to Equation 4,

$$\Delta G = \Delta G_{H_2O} - m\,[\text{GdmCl}] \quad \text{(Eq. 4)}$$

The biphasic transition of BAA was analyzed using a three-state model (22).

Dynamic Quenching of Fluorescence—The acrylamide-dependent quenching of intrinsic protein fluorescence was monitored in the presence of ~50 μg of enzyme (A_{280} <0.1) in a 1-ml initial volume of 30 mM MOPS, 50 mM NaCl, 1 mM $CaCl_2$, pH 7.2, at an excitation wavelength of 280 nm (1-nm band pass) and at an emission wavelength of 350 nm (2-nm band pass) after consecutive additions of 4 μl of 1.2 M acrylamide in the same buffer. The Stern-Volmer quenching constants K_{SV} were calculated according to the relation (23) shown in Equation 5,

$$F/F_0 = 1 + K_{SV}\,[\text{Q}] \quad \text{(Eq. 5)}$$

where F and F_0 are the fluorescence intensity in the presence and absence of molar concentration of the quencher Q, respectively. The intrinsic protein fluorescence F was corrected for the acrylamide inner filter effect f, the latter being defined as shown in Equation 6,

$$f = 10^{-\epsilon\,[\text{Q}]/2} \quad \text{(Eq. 6)}$$

using an extinction coefficient ϵ for acrylamide at 280 nm of 4.3 M^{-1} cm^{-1}.

Differential Scanning Calorimetry (DSC)—Measurements were performed using a MicroCal MCS-DSC instrument as detailed (12). Samples (~3 mg/ml) were dialyzed overnight against 30 mM MOPS, 50 mM NaCl, 1 mM $CaCl_2$, pH 7.2. Thermograms of enzyme-acarbose complexes were recorded in the presence of 1 mM acarbose (Bayer). Thermograms were analyzed according to a non-two-state model in which the melting point T_m, the calorimetric enthalpy ΔH_{cal}, and the van't Hoff enthalpy ΔH_{eff} of individual transitions are fitted independently using the MicroCal Origin software (version 2.9). The magnitude and source of the errors in the T_m and enthalpy values have been discussed elsewhere (24). Fitting standard errors on a series of three DSC measurements made under the same conditions in the present study were found to be ±0.05 K on T_m and ±1% on both enthalpies. Thermograms for equilibrium unfolding were recorded at 2 K min^{-1} and in the presence of 0.5 M 3-(1-pyridinio)-1-propanesulfonate for PPA and BAA. The thermodynamic parameters of unfolding were calculated using the relations (25) shown in Equations 7–9,

$$\Delta G(T) = \Delta H_{\text{cal}}(1 - T/T_m) + \Delta Cp(T - T_m) - T\Delta Cp\ ln(T/T_m) \quad \text{(Eq. 7)}$$

$$\Delta H(T) = \Delta H_m + \Delta\text{Cp}(\text{T} - \text{T}_\text{m}) \quad \text{(Eq. 8)}$$

$$\Delta S(T) = \Delta H_m/T_m + \Delta Cp\ ln(T/T_m) \quad \text{(Eq. 9)}$$

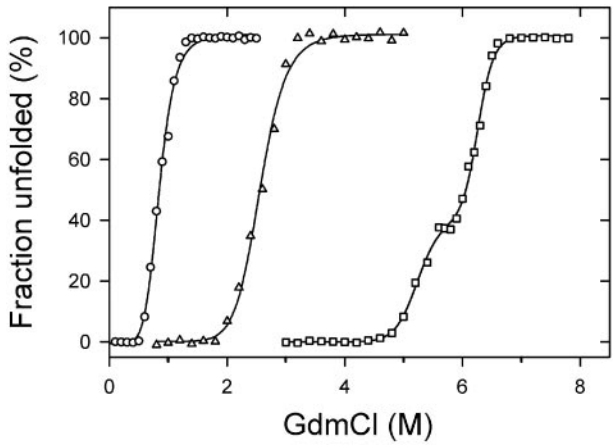

FIG. 1. **Equilibrium unfolding of the psychrophilic AHA (○), the mesophilic PPA (△), and the thermophilic BAA (□) as recorded by fluorescence emission.** Thermodynamic parameters of GdmCl-induced unfolding at 20 °C are as follows: for AHA, $C_{½}$ = 0.9 M, m = 4.3 kcal mol^{-1} M^{-1}, ΔG_{H_2O} = 3.7 kcal mol^{-1}; for PPA, $C_{½}$ = 2.6 M, m = 2.7 kcal mol^{-1} M^{-1}, ΔG_{H_2O} = 6.9 kcal mol^{-1}; for BAA, $C_{½}$ = 6.0 M, ΔG_{H_2O} = 23.8 kcal mol^{-1}. Reversibility was ≥85% for the three enzymes.

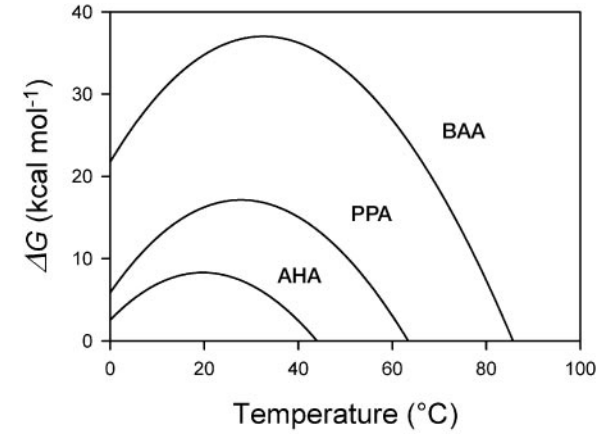

FIG. 2. **Gibbs free energy of unfolding.** Stability curves are shown for the psychrophilic AHA, the mesophilic PPA, and the thermophilic BAA, as calculated from microcalorimetric data (Equation 7).

with a heat capacity difference between the native and unfolded state ΔCp = 8.47 kcal mol^{-1} K^{-1} as determined experimentally (12). Kinetically driven unfolding was recorded at low scan rates (0.1, 0.5, and 1 K min^{-1}), and the rate constant k was calculated from the relation (26) shown in Equation 10,

$$k = vC_p/\Delta_{\text{cal}} - \Delta(T) \quad \text{(Eq. 10)}$$

where v is the scan rate, C_p is the excess heat capacity at a temperature T, Δ_{cal} is the total heat of the process, and $\Delta(T)$ is the heat evolved at a given temperature T.

RESULTS AND DISCUSSION

Conformational Stability—The stability of AHA, PPA, and BAA is illustrated in Fig. 1 by their GdmCl-induced unfolding transitions. These enzymes unfold at distinct denaturant concentrations ($C_{½}$) and are characterized by a decrease of unfolding cooperativity (m value) and the appearance of intermediate states (BAA) as the stability increases. These observations parallel the behavior of protein adapted to different temperatures as recorded by thermal unfolding (12, 13). Estimation of the conformational stability in the absence of denaturant (ΔG_{H_2O}) at 20 °C using Equation 4 provides a ratio of 1/2/6 for AHA, PPA, and BAA, respectively. The stability curves of the investigated enzymes have been calculated from DSC data using the modified Gibbs-Helmholtz equation (Equation 7).

TABLE I
Enthalpic and entropic contributions to conformational stability at relevant temperatures

α-amylase	At 0 °C			At T_{max}		At 37 °C		
	ΔG	ΔH	$T\Delta S$	T_{max}	$\Delta G = \Delta H$	ΔG	ΔH	$T\Delta S$
	kcal mol^{-1}	*kcal mol*$^{-1}$	*kcal mol*$^{-1}$	*°C*	*kcal mol*$^{-1}$	*kcal mol*$^{-1}$	*kcal mol*$^{-1}$	*kcal mol*$^{-1}$
AHA	2.5	−158.8	−161.3	20	8.3	4.1	154.7	150.6
PPA	5.9	−235.5	−241.4	30	17.1	16.0	76.5	60.5
BAA	21.7	−239.0	−260.7	33	37.0	36.7	74.4	37.7

TABLE II
Thermodynamic parameters for the irreversible heat inactivation of activity and for irreversible unfolding
As the three enzymes are denatured in different temperature ranges, activation data are reported for an identical rate constant, $k = 0.05\ s^{-1}$. Thermal unfolding data for AHA were obtained with the mutant N12R.

	Inactivation				Unfolding			
	ΔG^*	ΔH^*	$T\Delta S^*$	ΔS^*	ΔG^*	ΔH^*	$T\Delta S^*$	ΔS^*
	kcal mol^{-1}	*kcal mol*$^{-1}$	*kcal mol*$^{-1}$	*cal mol*$^{-1}$ *K*$^{-1}$	*kcal mol*$^{-1}$	*kcal mol*$^{-1}$	*kcal mol*$^{-1}$	*cal mol*$^{-1}$*K*$^{-1}$
AHA	20.5	172.3	151.8	479	20.2	109.7	89.2	286
PPA	21.5	153.0	131.5	395	21.5	84.7	63.2	190
BAA	22.9	58.6	35.7	101	22.9	74.2	51.3	145

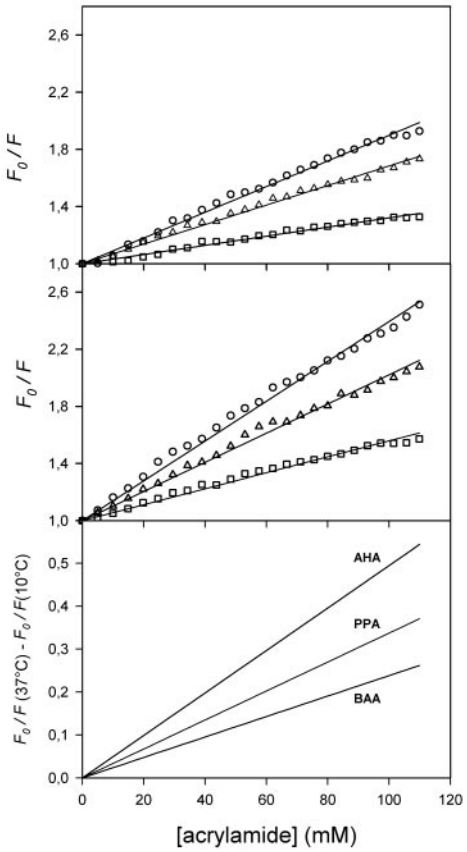

FIG. 3. **Stern-Volmer plots of fluorescence quenching by acrylamide.** Fluorescence quenching values at 10 °C (*upper panel*) and at 37 °C (*middle panel*) for AHA (○), PPA (△), and BAA (□) are shown. *Lower panel*, variation of fluorescence quenching between 10 and 37 °C obtained by subtracting the regression lines of Stern-Volmer plots at individual temperatures. The quenching constant K_{SV} values corresponding to the plot slope (Equation 5) are 0.90, 0.68, and 0.32 $mM^{-1} \cdot 10^{-2}$ at 10 °C and 1.39, 1.02, and 0.56 $mM^{-1} \cdot 10^{-2}$ at 37 °C for AHA, PPA, and BAA, respectively.

This function corresponds to the energy required to disrupt the native state at any temperature (27) and by definition is nil at the melting point (Fig. 2). The psychrophilic AHA unfolds reversibly according to a two-state mechanism, and the validity of its stability curve has been demonstrated by detection of the cold melting point predicted by the function (12). The poorly reversible thermal unfolding of PPA and BAA was analyzed according to the model of Lumry and Eyring, shown in Equation 11,

$$N \rightleftharpoons U \rightarrow I \qquad \text{(Eq. 11)}$$

using DSC data generated at fast scan rates (2 K/min) in the presence of a non-detergent sulfobetaine to prevent aggregation (28). In these conditions, it is assumed that the irreversible step has much lower enthalpy contribution and rate constant than the reversible step. As a result, the unfolding transition can be regarded to a first approximation as an equilibrium transition and can be treated by the equations of equilibrium thermodynamics (29, 30). Some general conclusions concerning the stability of extremophilic enzymes can be deduced from these curves. Despite large differences in melting point T_m, the ΔG_{max} values (top of the curve) are centered around room temperature, as anticipated from theoretical studies (31). Accordingly, the increasing melting points of the three enzymes are predominantly reached by lifting the stability curves. This is obtained by a corresponding increase of ΔH_{cal} in Equation 7 (at constant ΔCp), demonstrating the major involvement of enthalpic stabilization of the protein structure in temperature adaptation (32, 33). Furthermore, the analysis of these curves indicates that the heat-labile psychrophilic enzyme is also cold-labile, contrary to what is intuitively expected, whereas the heat-stable BAA is predicted to be the most cold-stable protein. The enthalpic and entropic contributions to ΔG have been calculated according to Equations 8 and 9 (Table I). The physiological temperatures for the heat-stable PPA and BAA lie on the right side of the bell-shaped ΔG curves, and therefore, their structure is stabilized enthalpically, whereas the thermal dissipative contribution of the unfavorable entropic term provides the required mobility for the enzyme function (25). In contrast, the physiological low temperatures for the psychrophilic enzyme lie on the left side of its stability curve. It follows that in environmental conditions, its structure is stabilized entropically, whereas the enthalpic contribution becomes a destabilizing factor. It is thought that hydration of polar and nonpolar groups is responsible for the decrease of stability at low temperatures, leading to cold unfolding (32, 34), and accordingly, this factor should contribute to the required mobility for function at environmental low temperatures.

Irreversible Unfolding and Heat Inactivation—Heat inactivation of activity was analyzed according to the kinetic model shown in Equation 12,

TABLE III
Activation parameters of the amylolytic reaction at 10 °C

α-amylase	k_{cat}	*Ea*	ΔG^*	ΔH^*	$T\Delta S^*$
	s^{-1}	*kcal mol*$^{-1}$	*kcal mol*$^{-1}$	*kcal mol*$^{-1}$	*kcal mol*$^{-1}$
AHA	294	8.9	13.8	8.3	−5.5
PPA	97	11.7	14.0	11.1	−2.9
BAA	14	17.4	15.0	16.8	1.8

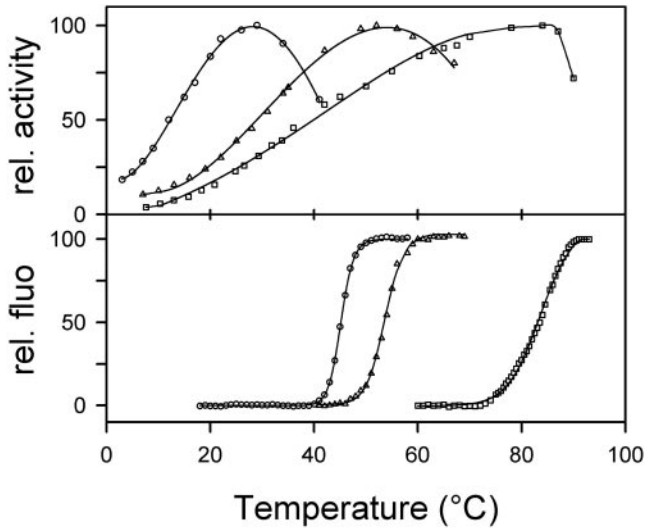

FIG. 4. **Temperature dependence of activity (*upper panel*) and of unfolding as recorded by fluorescence emission (*lower panel*).** Data for the psychrophilic AHA (○), the mesophilic PPA (△), and the thermophilic BAA (□) are provided. Experiments were performed at similar protein concentrations (5–40 μg/ml) in 100 mM Hepes, 50 mM NaCl, pH 7.2, in the absence of added Ca^{2+} (~1 μM residual Ca^{2+} as estimated by atomic absorption). Note also the decrease in unfolding cooperativity as the enzyme stability increases (*lower panel*).

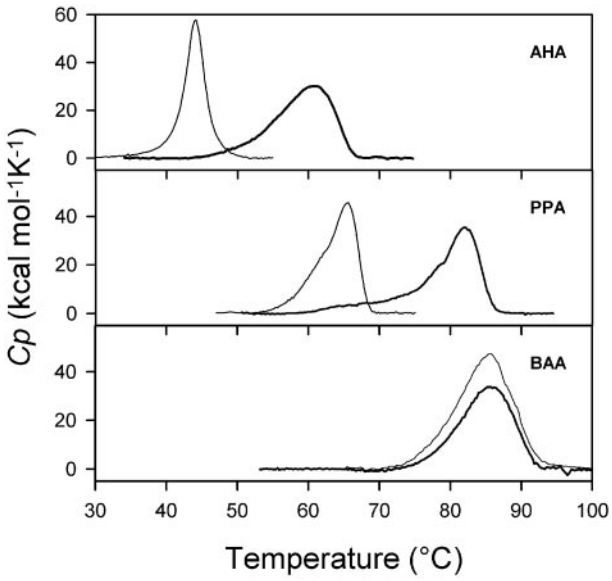

FIG. 5. **DSC endotherms of α-amylases in the free state (*thin lines*) and in complex with the transition state analog acarbose (*heavy lines*).** T_{max} corresponds to the top of the transition, and ΔH_{cal} corresponds to the surface below the transition (Table IV). Base line subtracted data have been normalized for protein concentration.

$$N \xrightarrow{k} I \qquad \text{(Eq. 12)}$$

and the activation parameters were calculated from Arrhenius plots. The irreversible conformational unfolding of PPA and BAA was analyzed from DSC data generated at low scan rates (<1 K/min). Such kinetic analysis is not possible for AHA (fully reversible unfolding), and data were obtained from its mutant N12R. The latter displays the same microcalorimetric properties as AHA but only 30% denaturation reversibility (13), ensuring that unfolding is kinetically driven. As a matter of fact, the melting point of the three enzymes is scan rate-dependent below 1 K/min, and the rate constant k was calculated from Equation 10. The corresponding activation parameters are provided in Table II, which shows that both heat inactivation of activity and irreversible unfolding of the structure display the same trends. The increase in free energy of activation from AHA to BAA reflects that the same denaturation rate constants k are reached at increasing temperatures (44, 60, and 80 °C for heat inactivation of AHA, PPA, and BAA, respectively). The small differences in ΔG^*, however, arise from large differences in the enthalpic and entropic contributions. Indeed, the lowest ΔG^* value for the psychrophilic enzyme corresponds to the largest ΔH^* and $T\Delta S^*$ contributions and conversely corresponds to the heat-stable BAA. The decrease of ΔH^* as enzyme stability increases mainly reflects the decrease in cooperativity of inactivation and of unfolding: for instance, the heat-labile AHA denatures in a shorter temperature range, leading to the sharp slope of the Arrhenius plots and subsequently to high activation energy *Ea* and ΔH^*. Such high cooperativity probably originates from the lower number of interactions required to disrupt the active conformation. In this formalism, $\Delta S^* > 0$ suggests that the randomness of the activated transition state increases before irreversible inactivation or unfolding. Accordingly, the transition state of the psychrophilic enzyme is reached through a larger entropy variation than that of BAA, possibly reflecting an increased disorder (of the active site or of the structure), which is the main driving force of heat denaturation. In addition, the thermophilic enzyme seems resistant to denaturation before the irreversible loss of activity and conformation (low ΔS^*). A thermophilic enzyme can then be regarded as an intrinsically stable protein that counteracts heat denaturation by a weak cooperativity of unfolding and inactivation. The entropy loss associated with hydration of nonpolar groups upon denaturation can also contribute to the differences in entropic contribution reported in Table II. In the case of unfolding, this is supported by the slight increase of hydrophobicity from AHA to BAA noted for these enzymes (12).

Conformational Flexibility and Protein Permeability—It is generally assumed that the increase in stability from psychrophilic to thermophilic proteins arises from a decrease in conformational flexibility (5, 25, 35–37). However, some experimental data do not fully support this theory (38–40), but it is also recognized that the time scale and motions possibly involved remain largely undefined (41). The conformational flexibility of the three investigated enzymes was probed by dynamic fluorescence quenching. Briefly, this technique utilizes increasing concentrations of a small quencher molecule (acrylamide in the present case) to probe the accessibility of tryptophane within a protein. The decrease of fluorescence arising from diffusive collisions between the quencher and the fluorophore reflects the ability of the quencher to penetrate the structure and can be viewed as an index of protein permeability

TABLE IV
Microcalorimetric parameters of thermal unfolding for α-amylases in the free state and in complex with the pseudosaccharide inhibitor acarbose

α-amylase	Free enzyme		Enzyme-acarbose complex		ΔT_{max}	$\Delta\Delta H_{cal}$
	T_{max}	ΔH_{cal}	T_{max}	ΔH_{cal}		
	° C	*kcal mol⁻¹*	*°C*	*kcal mol⁻¹*	*° C*	*kcal mol⁻¹*
AHA	44.0	214	60.6	304	16.6	90
PPA	65.6	295	81.9	306	16.3	11
BAA	85.7	427	85.7	347	0.0	−80

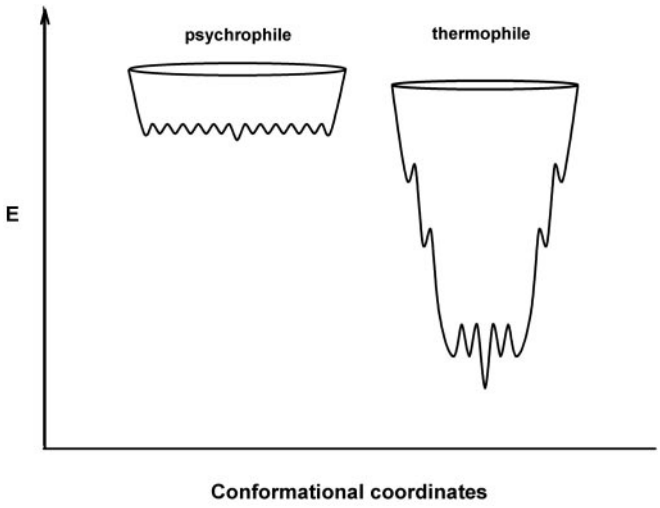

FIG. 6. **Proposed model of folding funnels for psychrophilic and thermophilic enzymes.** In these schematic energy landscapes, the free energy of folding or unfolding (*E*) is represented as a function of the conformational diversity, as detailed under "Conclusion."

(23). As illustrated in Fig. 3, this index significantly decreases from AHA to BAA (at 10 and 37 °C) and is inversely correlated with stability: the higher the stability, the lower the permeability. However, absolute values of the Stern-Volmer quenching constant (K_{SV}) can be compared only if the location of tryptophane residues in the structure is identical as well as their environment. This condition cannot be met for most closely related protein homologues (12, 19, and 17 Trp residues for AHA, PPA, and BAA, respectively), and therefore, the variation of these constants with temperature becomes the relevant parameter. Again, Fig. 3 shows that the variation of fluorescence quenching between 10 and 37 °C decreases in the order psychrophile → mesophile → thermophile. A similar variation was obtained between 10 and 25 °C (data not shown). Thus, the increase in protein permeability in a temperature range where the native state prevails is much larger for AHA, intermediate for PPA, and low for BAA. It should be noted that this permeability is the result of all conformational opening processes, averaged in a large time scale, allowing the quencher to diffuse into the protein. These data strongly support a correlation between stability and conformational flexibility.

Activity-Stability Relationships—It has been shown that the high activity at low temperatures of cold-adapted enzymes (corresponding to the low activation free energy ΔG^* of the reaction) mainly arises from low values of the activation enthalpy that render enzymatic reactions less temperature-dependent (42, 43). This is illustrated in Table III by the activation parameters of the three investigated enzymes. It has been further proposed that this property reflects the weak number of enthalpy-driven interactions that have to be broken to reach the transition state, leading to a heat-labile activity as these interactions also contribute to the active site conformation (20). As a first experimental approach, the thermodependence of the activity and the thermally induced unfolding transition were recorded in the same conditions, as shown in Fig. 4, in the absence of added Ca^{2+}, which stabilizes the structure (12) but inhibits the activity (44). In the case of the heat-stable PPA and BAA, the temperature for maximal activity closely corresponds to the fluorescence transition, showing that structural unfolding is a main determinant for the loss of activity at high temperatures. In contrast, the maximal activity of the psychrophilic enzyme is reached at about 30 °C, below any significant conformational event (Fig. 4). This shows that the active site of the psychrophilic enzyme (and the catalytic intermediates) is even more heat-labile than its protein structure. Such a result supports the concept of "localized flexibility" (43), which assumes that the low stability of the active site or of the structures bearing the active site is a main determinant of activity at low temperatures.

Table III also indicates that the magnitude of the entropic term of the enzymatic reaction decreases as the enzyme stability increases. It has been hypothesized that the flexible and mobile active site of psychrophilic enzymes undergoes larger structural fluctuations between the free and activated states than the more compact and rigid catalytic center of stable enzymes (20, 43). If this is true, and on the basis of the activation entropy (Table III), AHA trapped in the activated state should display larger structural differences with the free enzyme, PPA should display intermediate differences, and BAA should display minimal structural differences. To check this hypothesis, the stability of the three enzymes was recorded by DSC in the free state and in complex with acarbose, a large pseudosaccharide inhibitor acting as a transition state analog (16). Fig. 5 and Table IV reveal that upon acarbose binding, the psychrophilic enzyme is indeed strongly stabilized, as indicated by the large increases of the melting point and of the calorimetric enthalpy ΔH_{cal}. According to the same criterion, PPA is less stabilized in the transition state, whereas BAA is destabilized, as shown by the lower ΔH_{cal} value without melting point alteration. It is worth mentioning that both the magnitude and sign of these variations, as well as the macroscopic interpretation (assuming that a stabilized transition state intermediate is more ordered), parallels the structural fluctuations predicted by the activation entropy (Table III). These data strongly suggest that the improved activity at low temperatures of the psychrophilic enzyme is achieved by destabilizing the active site domain to reduce the temperature dependence of the activity (low ΔH^*), which in turn implies large structural motions upon substrate binding (high ΔS^*). The low activity of thermophilic enzymes at room temperature can be explained in the same way. The catalytic domain designed to be active at high temperature is stabilized by numerous interactions, resulting in a higher temperature dependence (high ΔH^*, and therefore, a low activity as the temperature decreases), whereas the moderate conformational changes of the rigid active site result in weak activation entropy variations.

Conclusion—These results and available data on enzymes adapted to extreme temperatures can be integrated in a model based on the "new view" using the folding funnel to describe the folding-unfolding reactions (45–48). Fig. 6 describes the energy landscape of psychrophilic and thermophilic enzymes. The

height of the funnel, *i.e.* the free energy of folding, also corresponding to the conformational stability, can be fixed in a 1/5 ratio according to the stability curves (Fig. 1, Table I). The upper edge of the funnels is occupied by the unfolded state in random coil conformations. It should be noted that psychrophilic enzymes tend to have a lower proline content than mesophilic and thermophilic enzymes, a lower number of disulfide bonds, and a higher occurrence of glycine clusters (8–11). Accordingly, the edge of the funnel for the psychrophilic protein is slightly larger (broader distribution of the unfolded state) and is located at a higher energy level. When the polypeptide is allowed to fold, the free energy level decreases, as well as the conformational ensemble. However, thermophilic proteins pass through intermediate states corresponding to local minima of energy. These minima are responsible for the ruggedness of the funnel slopes and for the reduced cooperativity of the folding-unfolding reaction as demonstrated by GdmCl and heat-induced unfolding. In contrast, the structural elements of psychrophilic proteins generally unfold cooperatively without intermediates, as a result of fewer stabilizing interactions and stability domains (12, 13), and therefore, the funnel slopes are steep and smooth. The bottom of the funnel, which depicts the stability of the native state ensemble, also displays significant differences between both extremozymes. The bottom for a very stable and rigid thermophilic protein can be depicted as a single global minimum or as having only a few minima with high energy barriers between them (49, 50), whereas the bottom for an unstable and flexible psychrophilic protein is rugged and depicts a large population of conformers with low energy barriers to flip between them. Rigidity of the native state is therefore a direct function of the energy barrier height (49, 50) and is drawn here according to the results of fluorescence quenching. In this context, the activity-stability relationships in these extremozymes depend on the bottom properties. Indeed, it has been argued that upon substrate binding to the association-competent subpopulation, the equilibrium between all conformers is shifted toward this subpopulation, leading to the active conformational ensemble (49–51). In the case of the rugged bottom of psychrophilic enzymes, this equilibrium shift only requires a modest free energy change (low energy barriers), a low enthalpy change for interconversion of the conformations, but is accompanied by a large entropy change for fluctuations between the wide conformer ensemble. The converse picture holds for thermophilic enzymes, in agreement with the activation parameters (Table III) and with the proposed macroscopic interpretation. Such energy landscapes integrate nearly all biochemical and biophysical data from extremophilic enzymes, but they will certainly be refined when other series of homologous proteins from psychrophiles, mesophiles, and thermophiles will become available.

Acknowledgments—We thank N. Gérardin and R. Marchand for skillful technical assistance and H. Bichoff (Bayer AG, Wuppertal, Germany) for the kind gift of acarbose.

REFERENCES

1. Sattler, B., Puxbaum, H., and Psenner, R. (2001) *Geophys. Res. Letters* **28,** 239–242
2. Vieille, C., and Zeikus, G. J. (2001) *Microbiol. Mol. Biol. Rev.* **65,** 1–43
3. Blochl, E., Rachel, R., Burggraf, S., Hafenbradl, D., Jannasch, H. W., and Stetter, K. O. (1997) *Extremophiles* **1,** 14–21
4. Deming, J. W. (2002) *Curr. Opin. Microbiol.* **5,** 301–309
5. D'Amico, S., Claverie, P., Collins, T., Georlette, D., Gratia, E., Hoyoux, A., Meuwis, M. A., Feller, G., and Gerday, C. (2002) *Philos. Trans. R. Soc. Lond. B Biol. Sci.* **357,** 917–925
6. Margesin, R., Feller, G., Gerday, C., and Russell, N. J. (2002) in *Encyclopedia of Environmental Microbiology* (Bitton, G., ed), Vol. 2, pp. 871–885, John Wiley and Sons, New York
7. Wintrode, P. L., and Arnold, F. H. (2000) *Adv. Protein Chem.* **55,** 161–225
8. Feller, G. (2002) *Cell. Mol. Life Sci.* **59,** in press
9. Gianese, G., Bossa, F., and Pascarella, S. (2002) *Proteins* **47,** 236–249
10. Russell, N. J. (2000) *Extremophiles* **4,** 83–90
11. Smalas, A. O., Leiros, H. K., Os, V., and Willassen, N. P. (2000) *Biotechnol. Annu. Rev.* **6,** 1–57
12. Feller, G., D'Amico, D., and Gerday, C. (1999) *Biochemistry* **38,** 4613–4619
13. D'Amico, S., Gerday, C., and Feller, G. (2001) *J. Biol. Chem.* **276,** 25791–25796
14. Aghajari, N., Feller, G., Gerday, C., and Haser, R. (1998) *Structure* **6,** 1503–1516
15. D'Amico, S., Gerday, C., and Feller, G. (2000) *Gene* (*Amst.*) **253,** 95–105
16. Qian, M., Haser, R., Buisson, G., Duee, E., and Payan, F. (1994) *Biochemistry* **33,** 6284–6294
17. Fitter, J., and Heberle, J. (2000) *Biophys. J.* **79,** 1629–1636
18. Fitter, J., Herrmann, R., Dencher, N. A., Blume, A., and Hauss, T. (2001) *Biochemistry* **40,** 10723–10731
19. Bernfeld, P. (1955) *Methods Enzymol.* **1,** 149–151
20. Lonhienne, T., Gerday, C., and Feller, G. (2000) *Biochim. Biophys. Acta* **1543,** 1–10
21. Pace, C. N. (1986) *Methods Enzymol.* **131,** 266–280
22. Grimsley, J. K., Scholtz, J. M., Pace, C. N., and Wild, J. R. (1997) *Biochemistry* **36,** 14366–14374
23. Lakowicz, J. (1983) *Principles of Fluorescence Spectroscopy*, pp. 257–301, Plenum Press, New York
24. Matouschek, A., Matthews, J. M., Johnson, C. M., and Fersht, A. R. (1994) *Protein Eng.* **7,** 1089–1095
25. Privalov, P. L. (1979) *Adv. Protein Chem.* **33,** 167–241
26. Sanchez-Ruiz, J. M., Lopez-Lacomba, J. L., Cortijo, M., and Mateo, P. L. (1988) *Biochemistry* **27,** 1648–1652
27. Privalov, P. (1992) in *Protein Folding* (Creighton, T., ed), pp. 83–126, W. H. Freeman and Company, New York
28. Vuillard, L., Braun-Breton, C., and Rabilloud, T. (1995) *Biochem. J.* **305,** 337–343
29. Privalov, P. L., and Medved, L. V. (1982) *J. Mol. Biol.* **159,** 665–683
30. Vogl, T., Jatzke, C., Hinz, H. J., Benz, J., and Huber, R. (1997) *Biochemistry* **36,** 1657–1668
31. Kumar, S., Tsai, C. J., and Nussinov, R. (2002) *Biochemistry* **41,** 5359–5374
32. Makhatadze, G. I., and Privalov, P. L. (1995) *Adv. Protein. Chem.* **47,** 307–425
33. Kumar, S., Tsai, C. J., and Nussinov, R. (2001) *Biochemistry* **40,** 14152–14165
34. Privalov, P. L. (1990) *Crit. Rev. Biochem. Mol. Biol.* **25,** 281–305
35. Kohen, A., Cannio, R., Bartolucci, S., and Klinman, J. P. (1999) *Nature* **399,** 496–499
36. Zavodszky, P., Kardos, J., Svingor, and Petsko, G. A. (1998) *Proc. Natl. Acad. Sci. U. S. A.* **95,** 7406–7411
37. Wrba, A., Schweiger, A., Schultes, V., Jaenicke, R., and Zavodsky, P. (1990) *Biochemistry* **29,** 7584–7592
38. Fields, P. A. (2001) *Comp. Biochem. Physiol. A Mol. Integr. Physiol.* **129,** 417–431
39. Svingor, A., Kardos, J., Hajdu, I., Nemeth, A., and Zavodszky, P. (2001) *J. Biol. Chem.* **276,** 28121–28125
40. Hernandez, G., Jenney, F. E., Jr., Adams, M. W., and LeMaster, D. M. (2000) *Proc. Natl. Acad. Sci. U. S. A.* **97,** 3166–3170
41. Jaenicke, R. (2000) *Proc. Natl. Acad. Sci. U. S. A.* **97,** 2962–2964
42. Low, P. S., Bada, J. L., and Somero, G. N. (1973) *Proc. Natl. Acad. Sci. U. S. A.* **70,** 430–432
43. Fields, P. A., and Somero, G. N. (1998) *Proc. Natl. Acad. Sci. U. S. A.* **95,** 11476–11481
44. Boel, E., Brady, L., Brzozowski, A. M., Derewenda, Z., Dodson, G. G., Jensen, V. J., Petersen, S. B., Swift, H., Thim, L., and Woldike, H. F. (1990) *Biochemistry* **29,** 6244–6249
45. Dill, K. A., and Chan, H. S. (1997) *Nat. Struct. Biol.* **4,** 10–19
46. Dobson, C. M., and Karplus, M. (1999) *Curr. Opin. Struct. Biol.* **9,** 92–101
47. Dinner, A. R., Sali, A., Smith, L. J., Dobson, C. M., and Karplus, M. (2000) *Trends Biochem. Sci.* **25,** 331–339
48. Schultz, C. P. (2000) *Nat. Struct. Biol.* **7,** 7–10
49. Tsai, C. J., Ma, B., and Nussinov, R. (1999) *Proc. Natl. Acad. Sci. U. S. A.* **96,** 9970–9972
50. Kumar, S., Ma, B., Tsai, C. J., Sinha, N., and Nussinov, R. (2000) *Protein Sci.* **9,** 10–19
51. Ma, B., Kumar, S., Tsai, C. J., Hu, Z., and Nussinov, R. (2000) *J. Theor. Biol.* **203,** 383–397